Supporting Information

for

Mobility-Controlled Performance of Thick Solar Cells based on Fluorinated Copolymers

Wentao Li,[#,1] Steve Albrecht,[#,2] Liqiang Yang,[3] Steffen Roland,[2] John R. Tumbleston,[4] Terry McAfee,[4] Liang Yan,[1] Mary Allison Kelly,[1] Harald Ade*,[4], Dieter Neher*,[2], and Wei You*[1,3]

 # equal contribution

corresponding authors: H.A (hwade@ncsu.edu), D.N. (neher@uni-potsdam.de), W.Y. (wyou@unc.edu)

1. Department of Chemistry, University of North Carolina at Chapel Hill
Chapel Hill, NC 27599-3290, USA.

2. Institute of Physics and Astronomy, Soft Matter Physics, University of Potsdam, 14476 Potsdam, Germany.

3. Department of Applied Physical Sciences, CB#3216, University of North Carolina, Chapel Hill 27599-3216, USA

4. Department of Physics, North Carolina State University, Raleigh, NC 27615, USA.

Table of Contents

General Methods:

<u>UV-visible spectra</u> were acquired on a Shimadzu UV-2600 spectrophotometer. The thin films for UV-visible measurement were coated from *o*-dichlorobenzene (ODCB) solution on pre-cleaned glass slides.

<u>Cyclic voltammetry</u> measurements were carried out using a Bioanalytical Systems (BAS) Epsilon potentiostat equipped with a standard three-electrode configuration. Typically, a three-electrode cell equipped with a glassy carbon working electrode, a $Ag/AgNO_3$ (0.01 M in anhydrous acetonitrile) reference electrode, and a Pt wire counter electrode were employed. The measurements were done in anhydrous acetonitrile with tetrabutylammonium hexafluorophosphate (0.1 M) as the supporting electrolyte under an argon atmosphere at a scan rate of 100 mV/s. Polymer films were drop cast onto the glassy carbon working electrode from a 2.5 mg/mL chloroform solution and dried under house nitrogen stream prior to measurements. The potential of $Ag/AgNO_3$ reference electrode was internally calibrated by using the ferrocene/ferrocenium redox couple (Fc/Fc^+). The electrochemical onsets were determined at the position where the current starts to differ from the baseline. The HOMO in electron volts was calculated from the onset of the oxidation potential (E_{ox}) according to the following equation:

$$HOMO = -[4.8eV + e(E_{ox} - E_{Fc/Fc^+})]$$

<u>Gel permeation chromatography (GPC)</u> measurements were performed on a Polymer Laboratories PL-GPC 220 instrument, using 1,2,4-trichlorobenzene as the eluent (stabilized with 125 ppm BHT) at135 °C. The obtained molecular weight is relative to polystyrene standards.

<u>^{1}H nuclear magnetic resonance (NMR)</u> spectra were obtained at 400 or 300 MHz as solutions in $CDCl_3$. Chemical shifts are reported in parts per million (ppm, δ) and referenced from tetramethylsilane.

SCLC hole mobility was acquired through the hole-only devices with a configuration of ITO/PEDOT:PSS/polymer:PCBM/MoO₃/Ag whereas the SCLC electron mobility was measured in the electron only devices with a configuration of ITO/PEIE/polymer:PCBM/Ca/Al. Polyethylenimine ethoxylated (PEIE) was used to prepare low work function electrode. [Zhou, Y., Fuentes-Hernandez, C., Shim, J., Meyer, J., Giordano, A. J., Li, H., Kippelen, B. *Science*, **2012**, *336(6079)*, 327–332. doi:10.1126/science.1218829] For the hole-only devices, the dark current densities J of polymer-PCBM blends were measured by applying a voltage between 0 and 10 V. These data were analyzed according to the Mott-Gurneys law using a Poole-Frenkel-type field-dependence of mobility:

$$J = \frac{9}{8}\varepsilon_r\varepsilon_0\frac{V^2}{d^3}\mu_o\exp(g\sqrt{V/d}),$$

where ε_0 is the permittivity of free space, ε_r is the dielectric constant of the polymer which is assumed to be around 3 for the conjugated polymers, μ_0 is the zero field mobility, V is the voltage drop across the device, and d is the film thickness of active layer. A weak Poole-Frenkel factor of $g = 1\cdot10^{-4}$ (cm/V)$^{1/2}$ was used without correcting the applied voltage for the built-in field or series resistance. For electron only devices, the applied voltage V was corrected from the built-in voltage V_{bi} and contact resistance V_r, which was found to be around 35 Ω from a reference device without the polymer layer. For electron only devices, dark current densities of polymer-PCBM blends were measured by applying a voltage from 0 to 6 V. The electron mobility was then calculated from the SCLC regime by fitting the $J^{0.5}$ vs. V curve according to Mott-Gurneys law:

$$J = \frac{9}{8}\varepsilon_r\varepsilon_0\mu\frac{V^2}{d^3}.$$

The synthesis of polymers started with the synthesis and purification of monomers (dibromo FTAZ , dibromo HTAZ and bistrimethyltin BnDT) and the purification of catalyst $Pd_2(dba)_3$ were as described in the previous publications. [Li, W.; Yang, L.Q.; Tumbleston, J. R.; Yan, L.; Ade, H.; You, W. *Adv. Mater.*, **2014** doi: 10.1002/adma.201305251] Polymerizations were conducted in a microwave reaction tube equipped with a stir bar, where the dibromo FTAZ and dibromo HTAZ with corresponding ratio, calculated amount of bistrimethyltin BnDT, P(*o*-tol)$_3$ and $Pd_2(dba)_3 \cdot CHCl_3$ were added. After three vacuum-argon refilling cycles, anhydrous o-xylene was added via syringe. The tube was then planted in a CEM Discover microwave reactor to allow the polymerization for 10 minutes (300 W, 200 °C, 100 psi, 10 minutes of heating time). The resulted gel was then dissolved in hot chlorobenzene and precipitated in methanol. The collected precipitation was extracted in a Soxhlet extractor by ethyl acetate, hexane, THF and chloroform subsequently. The chloroform portion was concentrated and precipitated in methanol again to yield a metallic-looking golden solid. The polymer yield: F00 (PBnDT-HTAZ): 84%, F25: 82%, F50: 81%, F75: 73%, and F100 (PBnDT-FTAZ): 83%.
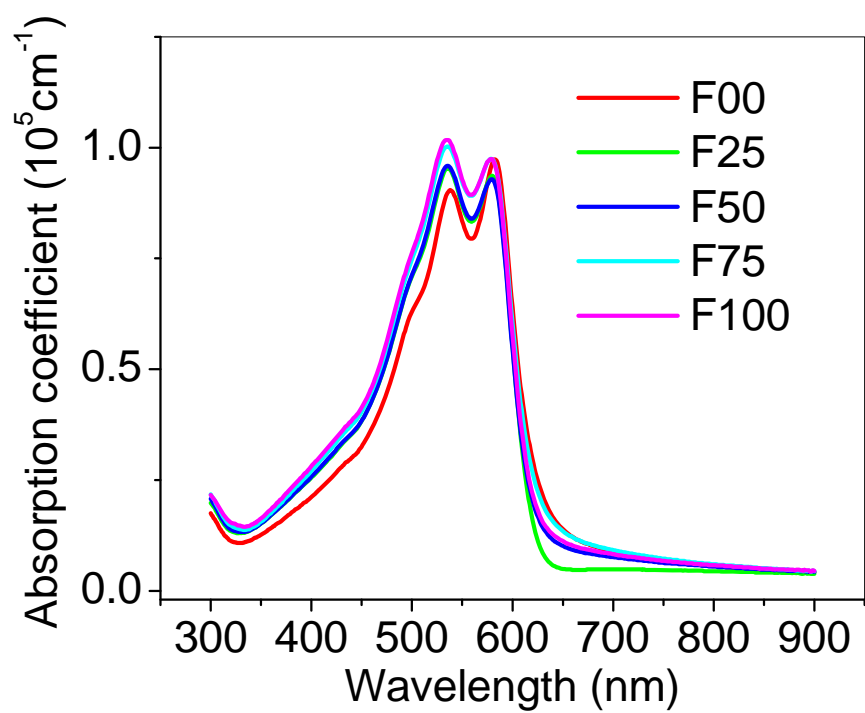
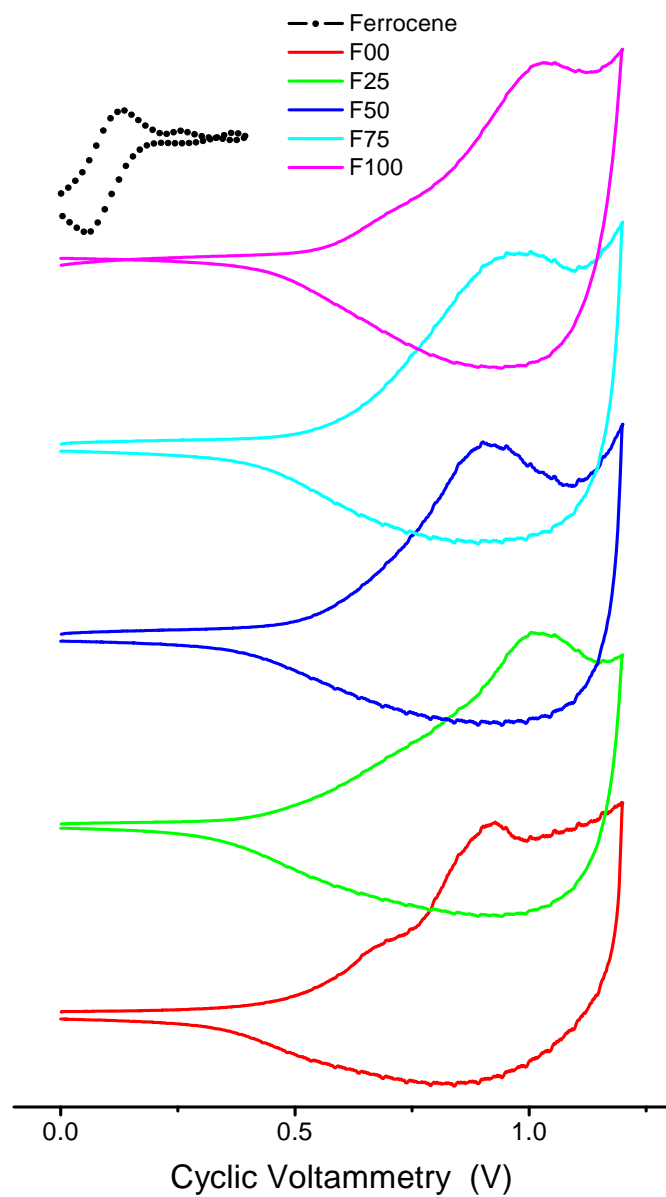**Figure S1. UV-Vis Absorption (Thin Film)**

Figure S2. Cyclic Voltammograms

Table S1. Estimated HOMO Energy Levels

Polymer	P3HT	F00	F25	F50	F75	F100
HOMO (eV)	-5.20	-5.38	-5.45	-5.39	-5.39	-5.45

Table S2. Detailed Device Data

PBnDT-FTAZ-FXX	Polymer : PCBM	Processing Solvent	Thickness (nm)	V_{oc} (V)	J_{sc} (mA/cm^2)	FF (%)	η (%)
F00*	1:2	TCB	347	0.731 ±0.004	11.27 ±0.48	46.6 ±0.9	3.84 ±0.16
F25	1:2	TCB	354	0.742 ±0.001	12.27 ±0.25	54.3 ±0.7	4.94 ±0.16
F50	1:2	TCB	340	0.764 ±0.002	12.44 ±0.37	62.3 ±1.0	5.92 ±0.22
F75	1:2	TCB	356	0.780 ±0.004	12.21 ±0.36	64.9 ±1.3	6.18 ±0.25
F100*	1:2	TCB	340	0.797 ±0.004	12.75 ±0.44	70.6 ±1.3	7.17 ±0.32

The thickness of the active layer is the average value from 3 measurements, with a typical error of ±10 nm.

Table S3. Estimated electron mobility via SCLC

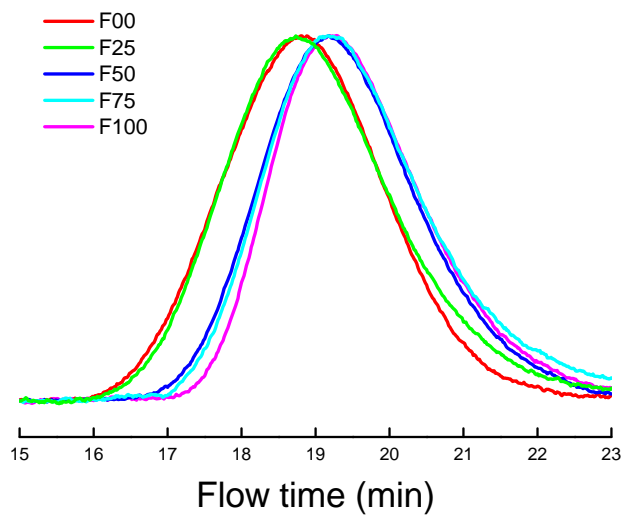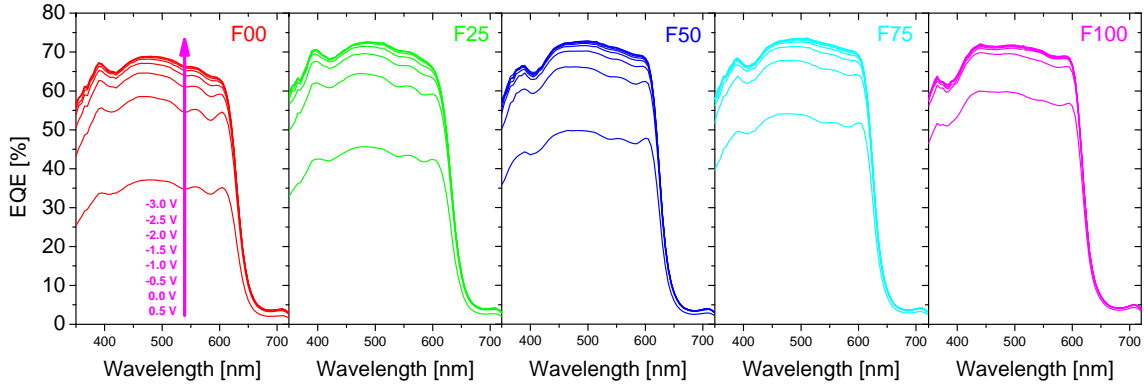| Polymer	F00	F25	F50	F75	F100
μ_e (10^{-3} cm^2/V·s)	5.4±2.2	3.2±1.5	6.7±2.9	3.4±0.9	2.9±0.8

Figure S3. GPC Curves

Figure S4. Field dependent EQE. EQE for different applied voltages ranging from +0.5V to -3V as indicated in the left plot.
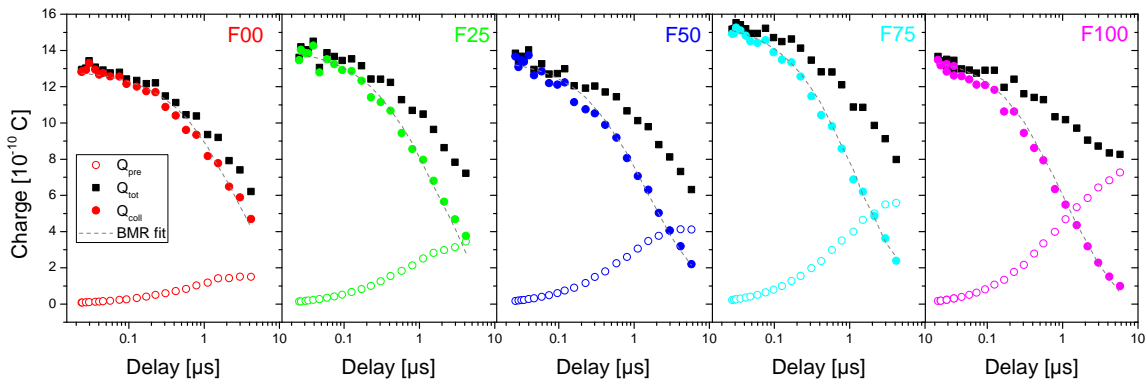

Figure S5. BMR coefficient. Time delay dependent charges extracted from TDCF measured at 0.7 V pre-bias for each blend with BMR fits as indicated by the dashed lines. Q_{pre} is the charge that can be extracted at the low internal field of the pre-bias. Q_{coll} is the charge that can be collected after the delay time and Q_{tot} is the sum of both.
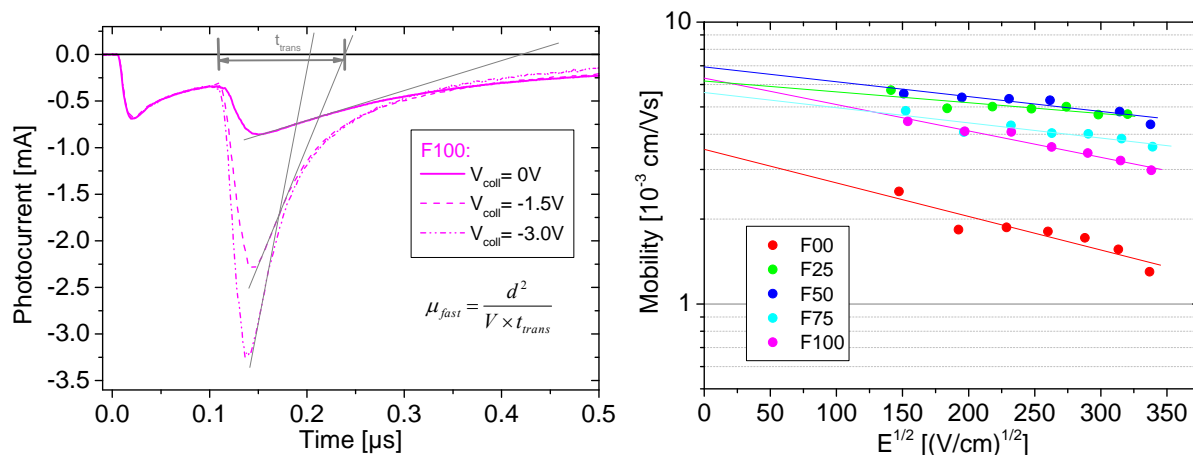
Figure S6. Mobility extracted from TDCF transients. Left: TDCF transients for different collection voltages. The Mobility of the faster type of carrier is determined from the extrapolation of the initial decay of the photocurrent to zero as exemplary shown for F100 blends. Right: The field-dependent mobilities for all five blends with extrapolation to zero field as shown in the left figure.
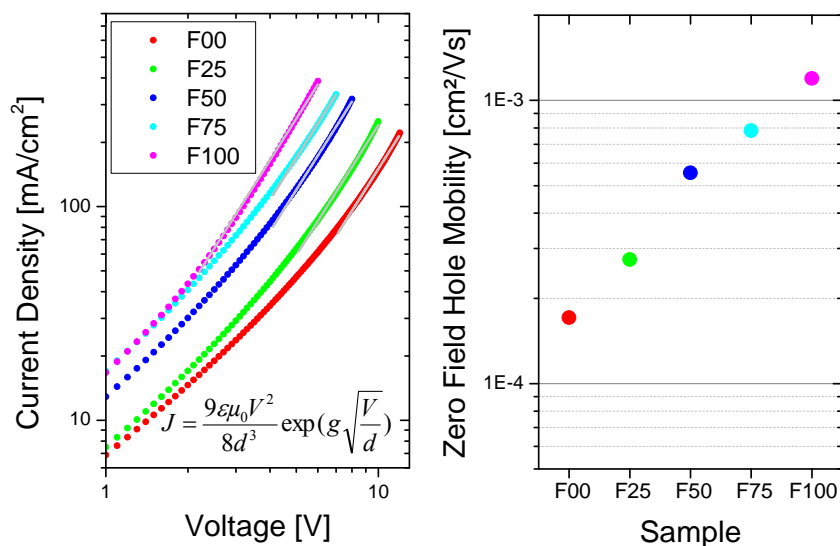

Figure S7. Hole mobility derived from the hole only devices. Left: Space charge limited currents of hole only devices with the fits according to Mott-Gurneys law using a Poole-Frenkel-type field-dependence of mobility (equation indicated) with a weak Poole-Frenkel factor to be $g = 1 \cdot 10^{-4}$ $(cm/V)^{1/2}$. Right: Zero field hole mobilities μ_0 deduced from the data in the left figure.
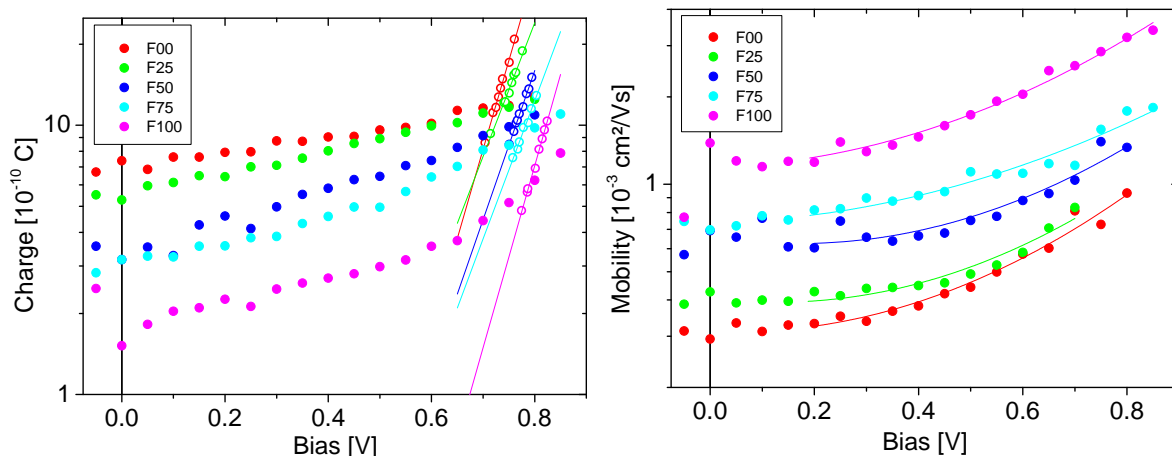
Figure S8. Carrier density and effective extraction mobility measured with BACE. Left: Carrier density measured with BACE with the intensity adjusted to give Jsc=14 mA/cm² for each blend (full circles) and the charge density at the respective open circuit voltage for each intensity (open circles) with linear fits for each blend. Right: effective extraction mobility as function of bias determined from the data in the left plot as described in the main text of the paper.
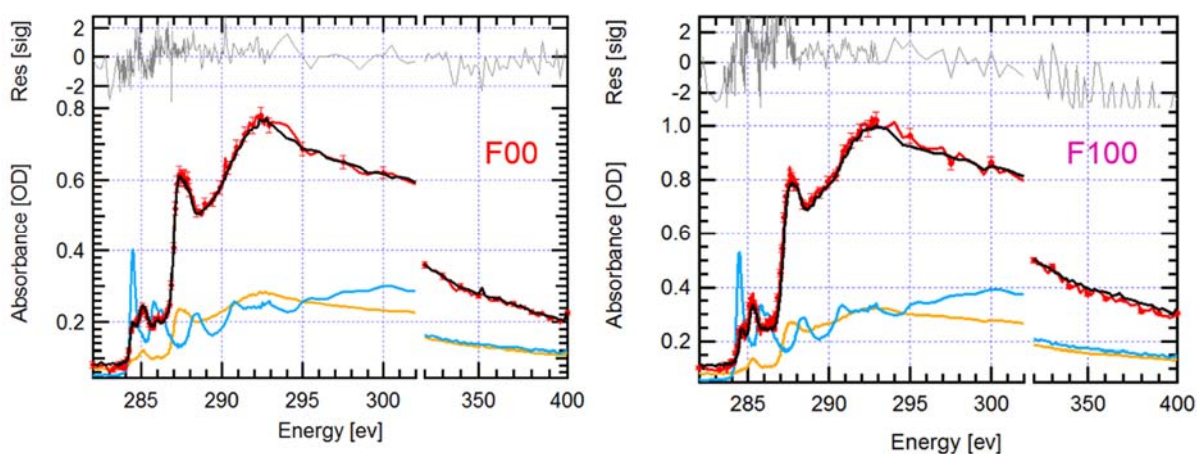

Figure S9. Molecular Miscibility. Scanning transmission X-ray microscopy scans of PCBM-depleted matrix after prolonged solvent anneal toward equilibrium. This annealing procedure results in large PCBM crystals formed by the PCBM (in the blends) that is in excess of the thermodynamic limit. Measurements in between these crystals thus reveal that only a residual of ~4% PCBM remains miscible in F00 (left) and F100 (right) polymers after solvent anneal in TCB. This indicates very low intrinsic miscibility between TAZ and PCBM with any level of fluorination. The low miscibility for F100 is in agreement with previous measurements: *Adv. Funct. Mater.* **23**, 3463-3470 (2013).
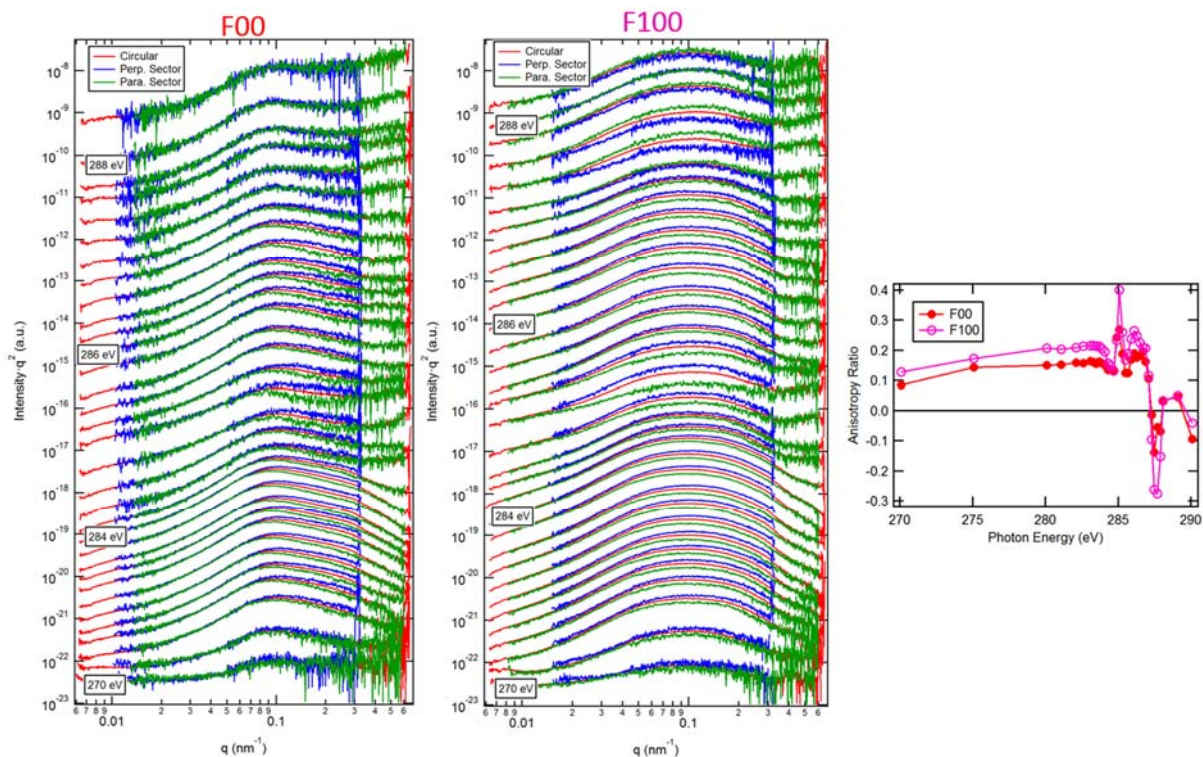
Figure S10. Scattering Anisotropy. Polarized soft X-ray scattering of F00 (left) and F100 (middle) blends as a function of incident photon energy from 270-290 eV (bottom to top). The 2D scattering data is reduced to circular, perpendicular (with respect to incident X-ray polarization), and parallel integrations. The upturn in scattering at high q is due to X-ray fluorescence and occurs for energies above the absorption energies of polymer and PCBM. The perpendicular and parallel integrations are further reduced to an anisotropy ratio (right) as described previously and is characteristic of these types of blends (Nat. Photon. **8**, 385-391 (2014)). Both blends show face-on molecular orientation with respect to donor/acceptor interfaces with the F100 blend showing a slightly higher degree of preferential orientation compared to the F00 blend.
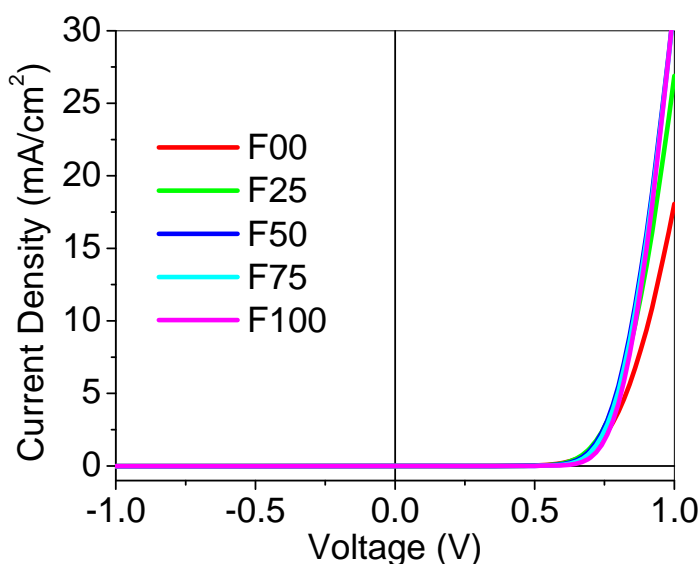
Figure S11 J-V curves in dark.
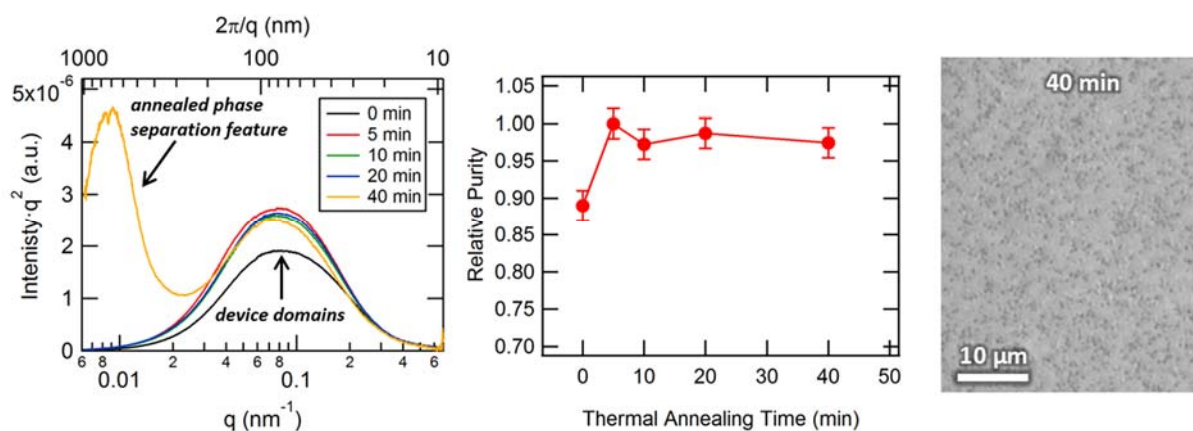
Figure S12. Thermal Anneal Sequence of F100 blend. P-SoXS data at 284.1 eV for F100 blend films thermal annealed at 150 C for different times. The relative purity determined from the TSI increases ~10% after 5 min of annealing indicating that the domains for the unannealed films in devices are not far from the equilibrium miscibility value (Figure S9). The visible light microscope image on the right shows micro-scale phase separation that begins between 20 and 40 min of annealing (as indicated from P-SoXS data).

NMR data

F00

8.219
7.334
7.259
4.871
3.199
3.187
3.163
3.148
3.116
3.102
1.920
1.587
1.527
1.399
1.385
1.161
1.148
1.130
1.073
1.063
1.001
0.987
0.961

2.00 4.08 0.71 3.31 1.19 3.75 66.74 20.06

F25

8.214
8.116
7.323
7.252
4.874
3.113
2.464
1.903
1.579
1.524
1.379
1.157
1.123
1.070
1.026

1.00 2.14 0.91 1.59 0.52 1.53 32.99 10.18

S15

F50

Peak labels: 8.175, 7.500, 7.333, 7.272, 4.879, 3.271, 3.266, 2.464, 1.953, 1.577, 1.526, 1.401, 1.384, 1.142, 1.117, 1.103, 1.059

Integration values: 1.00, 2.85, 0.43, 2.00, 0.64, 2.05, 40.02, 10.15

F75

Peak labels: 8.149, 8.136, 7.447, 7.334, 4.880, 3.250, 2.462, 1.946, 1.569, 1.516, 1.129, 1.091, 1.049

Integration values: 2.00, 5.70, 1.82, 3.31, 1.09, 3.43, 60.57, 20.24

F100